Conference paper

Giuseppina La Ganga* and Fausto Puntoriero

Artificial photosynthesis: a molecular approach to photo-induced water oxidation

Abstract: By the use of a molecular approach we performed photo-induced water oxidation by combining different photosensitizers and catalysts in order to obtain an efficient system that pave the way to the construction of an artificial photosynthetic system. Different types of molecular catalysts, such as ruthenium and vanadium polyoxometalates or cobalt core stabilized by different organic ligands were combined with ruthenium (II) polypyridine complexes of different nuclearity, mononuclear species like $[Ru(bpy)_3]^{2+}$ or a tetranuclear dendrimer.

Keywords: oxygen; photocatalysis; photosynthesis; XXV IUPAC Photochemistry.

DOI 10.1515/pac-2014-1106

Introduction

The development of artificial photosynthetic systems capable of efficiently converting light energy into chemical energy inspired by the photosynthetic process that is performed by natural organisms, is attracting a large degree of interest nowdays, for both fundamental and applicative reasons. Efficient artificial photosynthesis, aimed to produce high-energy content chemical species (i.e., fuels, like molecular hydrogen or carbon dioxide reduction products) from low-energy content chemical species (i.e., raw materials like water and CO_2), using solar energy as the energy source, would be a sort of Holy Grail of modern science [1–6], as it could solve problems connected with the intermittency and low-density of solar energy, since the sun light would be stored in chemical bonds, a convenient form of energy (storable, transportable, convertible) [7, 9, 10]. Moreover, solar energy is diffuse all over the world, and the social and political problems somehow connected with localization of fossil energy sources would be largely alleviated.

All schemes of artificial photosynthesis include water oxidation as a crucial step. In fact, water oxidation can be considered one of the major bottlenecks for achieving efficient artificial photosynthesis [11–13, 15]. As a consequence, in the last few years much work has been devoted to identify promising new catalysts for photoinduced water oxidation, and to integrate them into photosynthetic schemes. Herein we describe the development of photo-induced water oxidation in sacrificial schemes by combining different

Article note: A collection of invited papers based on presentations at the XXVth IUPAC Symposium on Photochemistry, Bordeaux, France, July 13–18, 2014.

***Corresponding author: Giuseppina La Ganga,** Dipartimento di Scienze Chimiche, Università degli Studi di Messina, via Ferdinando Stagno D'alcontres, 31 98166 Messina, Italy, Tel.: +00390906765136, Fax: +0039393756, E-mail: glaganga@unime.it

Fausto Puntoriero: Dipartimento di Scienze Chimiche, Università degli Studi di Messina, via Ferdinando Stagno D'alcontres, 31 98166 Messina, Italy

photosensitizers and catalysts. Different types of molecular catalysts, such as ruthenium and vanadium polyoxometalates or cobalt core stabilized by organic ligands were combined with ruthenium(II) polypyridine complexes of different nuclearity: mononuclear species like $[Ru(bpy)_3]^{2+}$ or a tetranuclear Ru(II) dendrimer. In particular, the tetranuclear Ru(II) photosensitizer allows for enhanced visible absorption properties accessing a large fraction of solar energy, including photons in the red region of the solar spectrum up to 720 nm.

Photo-induced water oxidation

Focusing on photo-induced water oxidation reaction and in order to realize an artificial system mimicking the oxygen evolving complex of PSII in natural photosynthesis, three fundamental components are strictly required, in a sacrificial scheme: (i) a photosensitizer, (ii) a catalyst, and (iii) the sacrificial agent.

A general scheme for photoinduced water oxidation is highlighted in eqs. 1–11, where P, SA and C are the photosensitizer, the sacrificial agent and the catalyst, respectively [16].

In eq. 1 *P, once formed by means of light, undergoes oxidative electron transfer in the presence of a primary acceptor, the sacrificial agent SA, leading to the formation of the oxidized photosensitizer, P^+ (eq. 2). *P, in eq. 3, decays back to its ground state P in a competitive reaction and the ratio between eqs. 2 and 3 rate constants determines the efficiency of P^+ production, which can be optimized (i.e., approaching 1) by adjusting the concentration of SA. A competitive poisoning reaction for the overall process is the back electron transfer between P+ and SA (eq. 4), which can be eliminated if SA rapidly decomposes upon reduction, as it is in the case of persulfate anion (eq. 5).

$$P + hv \rightarrow {}^*P \tag{1}$$

$${}^*P + SA \rightarrow P^+ + SA^- \tag{2}$$

$${}^*P \rightarrow P + hv' \text{ and/or heat} \tag{3}$$

$$P^+ + SA^- \rightarrow P + SA \tag{4}$$

$$SA^- \rightarrow \text{products} \tag{5}$$

$$P^+ + C \rightarrow P + C^+ \tag{6}$$

In presence of the catalyst C, the oxidized photosensitizer P^+ returns to its ground state P (and is ready for another cycle) together with the formation of the mono-oxidized catalyst, C^+ (eq. 6).

After consecutive stepwise oxidations of C^+ (eqs. 7–9), the C^{4+} species, i.e., the actual water oxidation catalyst (eq. 11), is formed.

$$P^+ + C^+ \rightarrow P + C^{2+} \tag{7}$$

$$P^+ + C^{2+} \rightarrow P + C^{3+} \tag{8}$$

$$P^+ + C^{3+} \rightarrow P + C^{4+} \tag{9}$$

$${}^*P + C^{n+} \rightarrow P^+ + C^{(n-1)+} \tag{10}$$

$$C^{4+} + 2\,H_2O \rightarrow C + O_2 + 4\,H^+ \tag{11}$$

Thermodynamic factors are expected to be different for the various stepwise monooxidation processes shown in eqs. 6–9. Equation 10 is another poisoning reaction, which can involve any C^{n+} species (with n = 1–3) and could compete with eq. 2, but keeping the concentration of C low can minimize it.

It is worth noting that in the above scheme, it is implicitly assumed that SA is a chemical species; but a semiconductor electrode can also assume this role [22]. In this latter case, the optimization of reaction 2 vs. reaction 3 s can be obtained by modifying the level of the semiconductor conduction band by an applied bias.

The irreversibility of the overall process is given, rather than by eq. 5, by removal of the negative charge from SA^- via an external circuit.

A favorable interplay of rates governing each of the processes described above becomes a stringent requirement for high performance of a photo-induced water oxidation system. In particular fast electron transfer, after consecutive light absorption/charge separation events, should occur from the catalyst to the generated "hole" in order to override any backward electron flux while scavenging the nascent oxidant site and preserving the sensitizer structure. This is one of main conditions required to obtain a high performance system under a catalytic regime.

Time-resolved spectroscopic experiments are instrumental to address electron transfer kinetics and, interfacial communication between the light-activated oxidant and the metal cluster donor. More so, the screening of the catalyst performance under light activation by the sacrificial oxidant "shortcut" is a revealing tool in this search. This is best performed by combination of a water soluble photoactive unit, P, with a sacrificial oxidant SA, offering a suitable thermodynamic sink.

In many examples reviewed in the last years, the ruthenium(II) polypyridyl sensitizer $Ru(bpy)_3^{2+}$ (bpy = 2,2′-bipyridine) is generally coupled with either persulfate, $S_2O_8^{2-}$, or $Co(NH_3)_5Cl^{2+}$ as sacrificial acceptors. Under such conditions, the problem of electron back-donation is generally ruled out as the ideal terminal acceptor undergoes irreversible decomposition after electron injection.

Therefore, the screening of selected antennas/photoreaction center/catalysts under sacrificial acceptor conditions offers a valid hint on the one-way electron communication/flow within the assembly, enabling the optimization of the individual tasks [18].

Photoinduced water oxidation with a tetranuclear ruthenium sensitizer and a ruthenium polyoxometalate as catalyst: a unique 4 × 4 ruthenium interplay

In an efficient photo-induced water oxidation cycle, the photosensitizer plays an important role so that it must have essential properties: i) it has to absorb as much visible light as possible, ii) its oxidized state has to undergo a fast and efficient photo-induced electron transfer with the catalyst and iii) the oxidized sensitizer must have a suitable potential to allow the hole accumulation on the catalyst.

In recent years, in the literature [15–23, 26], many examples report on the use of $[Ru(bpy)_3]^{2+}$ as photosensitizer in light induced water oxidation cycle, but the limited absorption in the visible region of this chromophore is a serious drawback for its use as a sensitizer. In order to take full advantage of solar radiation, sensitizers having a larger cross section with solar light are desired.

With this aim, we identified a first-generation dendrimer, $[Ru\{(\mu\text{-dpp})Ru(bpy)_2\}_3](PF_6)_8$, **($Ru_4$dendrimer)** (bpy = 2,2′-bipyridine; dpp = 2,3-bis(2′-pyridyl)pyrazine), with enhanced visible absorption properties. Actually, **Ru_4dendrimer** belongs to the class of supramolecular light-harvesting antennas featuring significant absorption throughout a large portion of the visible region [24, 25]. **Ru_4dendrimer** enables photocatalytic water oxidation by IrO_2 in the presence of persulfate as sacrificial acceptor, under light irradiation with λ up to 700 nm and quantum yield ($\Phi=O_2$ moles/moles of absorbed photons) around 0.015. Notably, **Ru_4dendrimer** works at a wavelength where classical $[Ru(bpy)_3]^{2+}$-type compounds are totally ineffective [29].

So we turned our attention to the fully inorganic oxygen evolving complex $[Ru_4(\mu\text{-}O)_4(\mu\text{-}OH)_2(H_2O)_4(\gamma\text{-}SiW_{10}O_{36})_2]^{10-}$, **$Ru_4$POM** (POM stands for polyoxometalate) (Scheme 1), exhibiting a multi-turnover efficiency and fast kinetics. **Ru_4POM** is a highly robust polyanion, in which the tetra-Ru(IV)μ-oxo core mimicks the oxygen-evolving complex of natural photosynthesis by undergoing four consecutive oxidation steps, before releasing oxygen [22, 30]. The performance of **Ru_4POM** as a water oxidation catalyst has been demonstrated in the dark conditions [22, 23], and by using $[Ru(bpy)_3]^{2+}$ as a sensitizer in the presence of sacrificial acceptors [22, 32]. Evidence of a very fast hole scavenging process for photogenerated $[Ru(bpy)_3]^{3+}$ by **Ru_4POM** has been recently obtained with time-resolved spectroscopy, yielding a diffusion-controlled electron transfer rate (ns timescale) [33]. This result is instrumental in overcoming the slowness of hole scavenging processes associated with the use of IrO_2 nanoparticles [23].

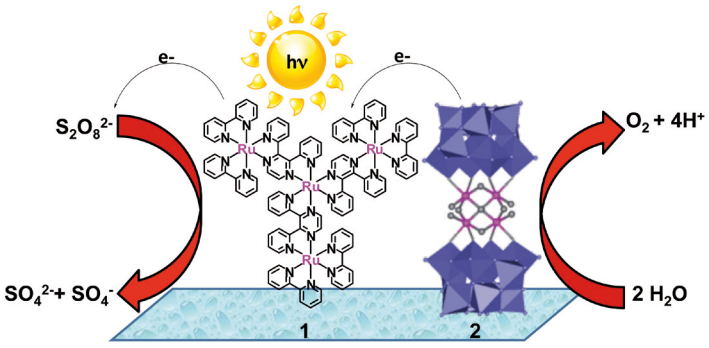

Scheme 1: Schematic representation of photocatalytic water oxidation by the interplay of tetra-ruthenium sensitizer/catalytic sites of **Ru_4dendrimer** and **Ru_4POM** in homogeneous solution. Reproduced from ref. [36] with the permission of the Royal Society of Chemistry.

The photo-induced water oxidation system developed with **Ru_4dendrimer** as photosensitizer and **Ru_4POM** as catalyst by using persulfate as sacrificial acceptor and operating at pH 7, in phosphate buffer solution (see Scheme 1), leads to oxygen evolution with an unprecedented photon-to-oxygen quantum yield, $\Phi = 0.30$, at an excitation wavelength of 550 nm [36].

Figure 1 shows the time-profile of oxygen evolution during continuous irradiation of the **Ru_4dendrimer**/**Ru_4POM**/$S_2O_8^{2-}$ system: linear kinetics is maintained up to ca. 80 % reaction within the overall experimental time (180 min). The dependence of the amount of O_2 so obtained was measured using a method already described [29]. In this time-frame, the chemical yield (CY) of the process, assumed as the amount of molecular oxygen produced on the basis of the amount of the persulfate, is 90 % (average yield over three runs); so the process is almost quantitative. Similar results are obtained by using different buffers and pH conditions (Na_2SiF_6, 2.6×10^{-3} M/$Na_2B_4O_7$, 1.14×10^{-2} M; pH = 5.8) [36].

A direct comparison with catalysis by the **Ru_4dendrimer**/malonate-stabilized IrO_2 nanoparticles/ $S_2O_8^{2-}$ system is reported in Fig. 1. It can be noted that colloidal IrO_2 displays a significantly lower efficiency in terms of both rate and O_2 yield with a CY of 15 % and a quantum yield of 0.05. This has been attributed to the degradation of the photosensitizer, occurring by competing pathways after excitation [27–29].

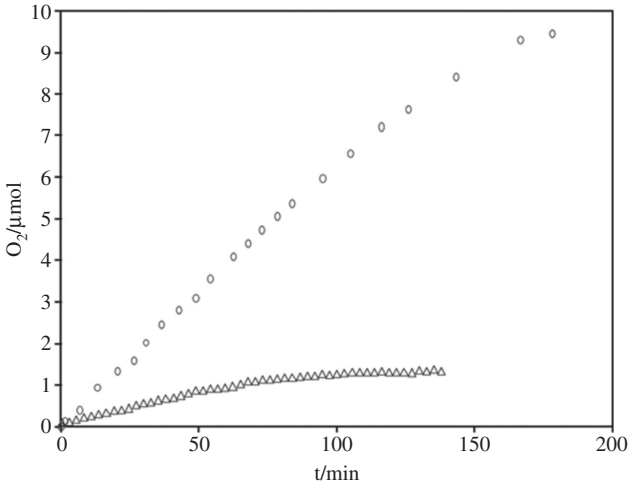

Fig. 1: Photocatalytic oxygen evolution as a function of time ($\lambda_{irr} > 550$ nm) observed in a buffered water solution (KH_2PO_4, 1×10^{-2} M, pH = 7.2) in the presence of **Ru_4dendrimer** (1×10^{-4} M), $Na_2S_2O_8$ (1×10^{-2} M) and **Ru_4POM** (as lithium salt, 6×10^{-5} M, circles;), or IrO_2 nanoparticles (6×10^{-5} M in iridium oxide content, triangles). Reproduced from ref. [36] with the permission of the Royal Society of Chemistry.

Catalyst **Ru_4POM** turns out to scavenge the oxidized ruthenium-centered sensitizer, with a rate constant on the ns timescale when the sensitizer is $[Ru(bpy)_3]^{2+}$. Based on thermodynamics, and assuming that all the involved processes occur in the Marcus normal region of classical electron transfer theory, the sequential hole scavenging processes of the oxidized sensitizer by **Ru_4POM**, ultimately yielding the **Ru_4POM^{4+}**, are expected to be faster for **Ru_4dendrimer** (whose oxidation potential falls at +1.55 V vs. SCE) than for $[Ru(bpy)_3]^{2+}$ (oxidation potential, +1.26 V vs. SCE) [19]. Whereas this hypothesis needs to be directly verified by ultrafast spectroscopy, very fast hole scavenging processes of the oxidized sensitizer would have the dual function of increasing the efficiency of the overall process and protecting the photosensitizer from photoinduced decomposition. In fact, comparison between the absorption spectra of the solution before and after the process (Fig. 2) indicates that only minimal changes takes place, suggesting a sensitizer decomposition ≤5 % [36].

The quantum yield of oxygen production by the **Ru_4dendrimer/Ru_4POM/**$S_2O_8^{2-}$system results $\Phi = 0.30$ ($\pm$ 0.03); this is significantly larger than the literature $\Phi = 0.045$ reported for $[Ru(bpy)_3]^{2+}$ as photosensitizer with **Ru_4POM** as catalyst [22, 32]. Although the complete mechanistic picture is yet to be clarified, the increase in light conversion efficiency by almost one order of magnitude is likely ascribed to an enhanced robustness and stability of the photochemical system. In this matter, the predicted faster hole-scavenging involving the oxidized sensitizer and the various oxidation states of **Ru_4POM** along the multistep route to prepare **Ru_4POM^{4+}** can play a key role.

On the basis of the experimentally determined Φ, 60 % of the absorbed photons are herein used to produce oxygen.

This great result could be implemented searching for earth abundant substitutes for ruthenium and iridium. This search is a fundamental target towards WOC sustainability and energy economy.

Photo-induced water oxidation by using cobalt cubane as catalyst

Due to the research into water oxidation catalysts based on earth-abundant elements in the last few years, there has been renewed interest in molecular cobalt species as water oxidation catalysts. Nevertheless, only a few examples of the molecular cobalt WOCs reported have actually been used to activate photocatalytic cycles [14, 34–37].

Among molecular catalysts studied, the cubane-shaped complex, with formula $[Co^{III}_4(\mu\text{-}O)_4(\mu\text{-}CH_3COO)_4(p\text{-}NC_5H_5)_4]$ (Co_4O_4-H, Fig. 3) deserved particular attention since (i) cobalt is a low-cost and abundant metal, (ii) its tetranuclear oxo core mimics the natural oxygen-evolving complex of Photosystem II [38–40], and (iii) it stands as the homogeneous analogue of the amorphous cobalt oxide/hydroxide film (Nocera's catalyst, sometimes referred to as Co-Pi) [41], whose electrocatalytic potential has been recently exploited within light activated devices [42–44].

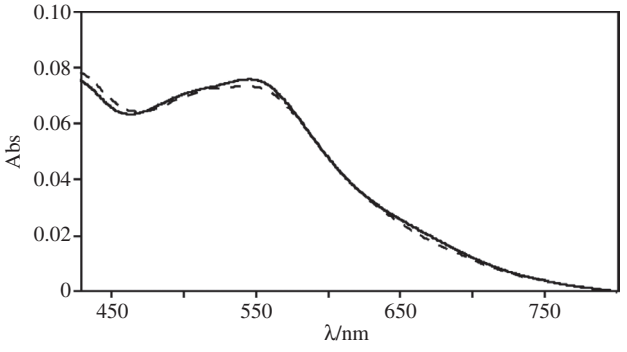

Fig. 2: Absorption spectra of buffered water solutions containing **Ru_4dendrimer**, **Ru_4POM**, and persulfate sacrificial agent before (solid line) and after 180 min of light irradiation (dashed line). The spectral range shown corresponds to the lowest-energy MLCT bands of the photosensitizer. Decomposition of the photosensitizer is estimated from the reduction of its absorption at 550 nm. Reproduced from ref. [36] with the permission of the Royal Society of Chemistry.

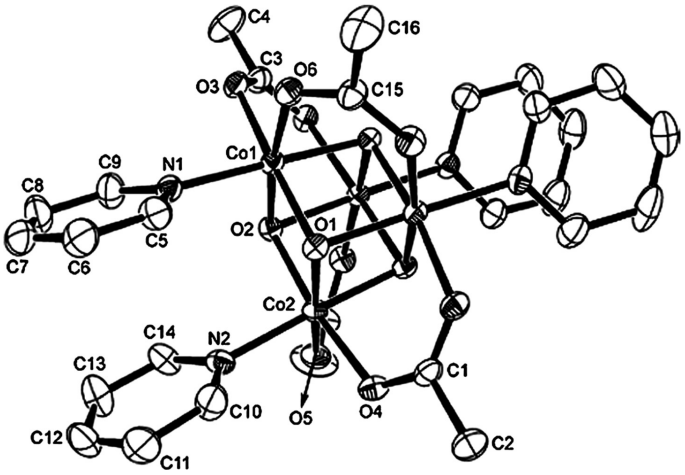

Fig. 3: X-ray structure of molecular cubane $[Co^{III}_4(\mu\text{-}O)_4(\mu\text{-}CH_3COO)_4(p\text{-}NC_5H_5)_4]$ (**Co_4O_4-H**). Reproduced from ref. [38] with the permission of the Royal Society of Chemistry.

Photoinduced water oxidation to molecular oxygen takes place in system where $[Ru(bpy)_3]^{2+}$ is the photosensitizer, Co_4O_4–H the molecular catalyst and $Na_2S_2O_8$ the sacrificial electron acceptor. Photocatalytic oxygen evolution as function of time, as well as the stability of the system, were measured by checking absorption spectral changes in the UV-Vis range before and after irradiation [39].

The photochemical quantum yield of the process reached the outstanding value of 0.3 ± 0.03 under experimental conditions described above (Fig. 4, excitation at 450 nm, irradiation time <10 min, when oxygen production is roughly linear) and depends on pH and catalyst concentration.

While the photochemical quantum yield for water oxidation by Co_4O_4–H in buffered solutions was promising; the same cannot be said for the chemical yield (CY) of the process. In fact, in the experiment shown in Fig. 4, CY is 28 % of the theoretical amount of oxygen that could be obtained.

The main reason for this behavior is the decomposition of the photosensitizer, which leads to deactivation of the catalytic process [40]. Indeed, the absorption spectrum of the catalytic mixture after 30 min of irradiation clearly indicates that the ruthenium sensitizer has been modified (Fig. 5). The changes of the absorption spectra agree with progressive decomposition of the photosensitizer. According to literature [45, 46], such a decomposition is attributed to reactions of the oxidized sensitizer, which, although not fully clarified, most probably involves nucleophilic attack, possibly by OH^- on the $[Ru(bpy)_3]^{3+}$ species.

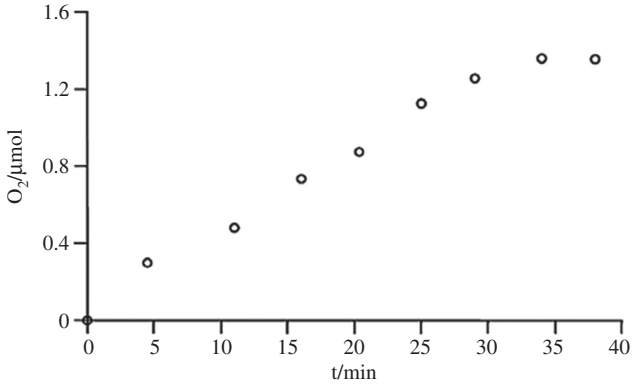

Fig. 4: Photocatalytic oxygen evolution as a function of time from a 2 mL solution of Co_4O_4–H (1.87×10^{-5} M) containing $[Ru(bpy)_3]^{2+}$ (1 mM) and $Na_2S_2O_8$ (5 mM), at pH 8 in 80 mM borate buffer, upon light irradiation ($\lambda > 400$ nm). Reproduced from ref. [39] with the permission of the Royal Society of Chemistry.

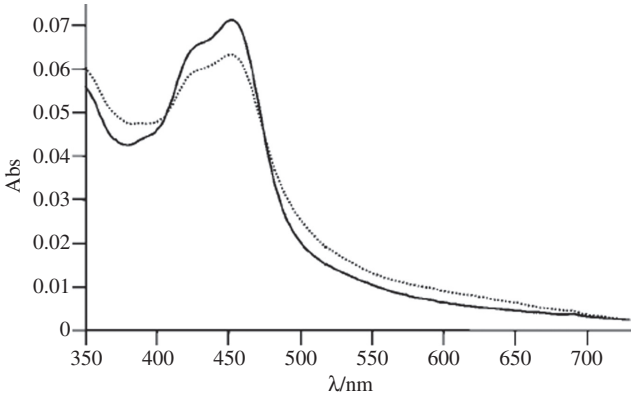

Fig. 5: Absorption spectral changes (visible region) of the photoirradiated solution before (solid line) and after (dotted line) the photocatalytic process.

To have experimental information on the rate constant of the hole scavenging process involving $[Ru(bpy)_3]^{3+}$ and Co_4O_4–H, we performed transient absorption spectroscopy.

These experiments indicate that: (i) the rate constant of the hole scavenging does not change significantly between pH 7 and 8; and (ii) hole scavenging is always significantly faster than the slow decomposition of the oxidized photosensitizer (reported to be of the order of 10^{-3}–10^{-2} s^{-1}, not detectable in the time scale of the flash photolysis experiments) [39].

The system $[Ru(bpy)_3]^{2+}$/ Co_4O_4–H/ $Na_2S_2O_8$ was investigated in more detail and, in particular, the effect of catalyst concentration on the photocatalytic activity was monitored. Photochemical quantum yield and the chemical yield of the system were collected in different experimental conditions: at pH 7 and at pH 8, by keeping constant other parameters (sensitizer concentration, light irradiation, buffer concentration) as it is shown in Table 1.

Focusing on the data collected in Table 1, a clear decrease in the photocatalytic activity of the system occurs on passing from pH 8 to pH 7, when sensitizer and catalyst concentrations are kept constant. In these latter conditions ($[Ru(bpy)_3^{2+}] = 1$ mM, $[Co_4O_4–H] = 1.87 \times 10^{-5}$ M), in fact, the photochemical quantum yield of oxygen production decreases to 0.10, although the chemical yield has not changed. At first sight, the reason for such a decreased photochemical quantum yield at pH 7 could be attributed to the potential E_{ox} for water oxidation, which increases from +0.76 V at pH 8 to +0.82 V at pH 7 so, as a consequence, water oxidation becomes less favorable from a thermodynamic viewpoint.

Moreover, when the concentration of Co_4O_4–H is doubled, on passing from 1.87×10^{-5} M to 3.75×10^{-5} M, at pH 8 the photochemical quantum yield decreases from 0.30 to 0.20, whereas the chemical yield increases

Table 1: Photocatalytic behavior of the investigated system containing $[Ru(bpy)_3]^{2+}$ (1 mM), Co_4O_4-H and $Na_2S_2O_8$ (5 mM) in borate buffer 80 mM (pH = 8) and in phosphate buffer 40 mM (pH = 7).

Catalyst concentration	pH8		pH7	
	Φ	CY	Φ	CY
10×10^{-5} M	0.20	46 %		
7.86×10^{-5} M	0.23			
5.65×10^{-5} M	0.21			
3.75×10^{-5} M	0.2	34 %	0.17	50 %
3.00×10^{-5} M	0.27			
1.87×10^{-5} M	0.30	28 %	0.10	30 %
1.00×10^{-5} M	0.25			
0.5×10^{-5} M	0.18			

Φ and CY at pH 7 for the lowest catalyst concentration were not determined.

to 34 %. Different trends are found by operating at pH 7, where increasing catalyst concentration from 1.87×10^{-5} M to 3.75×10^{-5} M leads to a higher quantum yield (from 0.10 to 0.17) and also induces an increase in chemical yield (from 30 % to 50 %). So it is clear that the photochemical quantum yield maximizes at concentration of catalyst of about 2×10^{-5} M at pH 8 and of about 8×10^{-5} M at pH 7.

The detailed mechanism of the photocatalytic process with the tetracobalt(III) cubane Co_4O_4–H is not known, but presumably must involve intermediate species with Co(IV) active sites, analogous to the Co–Pi system (Nocera's catalyst) [47]. In this case, some kind of reaction involving such intermediate species could play the role of self-poisoning reactions, removing the C^{n+} species from the catalytic process, leading to a decreased photochemical quantum yield of the overall process on increasing Co_4O_4–H concentration. Note that, while the poisoning reactions do not lead to catalyst decomposition, these parasite routes would affect the kinetic of O_2 production (therefore Φ), but not the chemical yield. Within this general picture, many details of the mechanism remain to be explained. In particular, the complex pH dependence by which the relative ordering of quantum yields for O_2 production at pH 8 and pH 7 would be reversed at a catalyst concentration of about 4×10^{-5} M, should be regarded, for the moment, as an empirical, practically relevant observation.

The photoinduced water oxidation abilities of the $[Ru(bpy)_3]^{2+}/Co_4O_4$–H/$Na_2S_2O_8$ system were significantly improved on changing solvent, passing to a mixed acetonitrile/aqueous borate buffer solution (buffer concentration, 10 mM, pH 8) [48]. In this mixed solvent, the reduction potentials of the $[Ru(bpy)_3]^{3+}/[Ru(bpy)_3]^{2+}$ and Co_4O_4–H $^{+}/Co_4O_4$–H redox couples were 1.20 and 0.93 V vs. Ag/AgCl, respectively, so a more favorable driving force for the hole scavenging was obtained. Indeed, under these conditions the hole scavenging process was quantitative, with a pseudo-first order rate constant, 1.3×10^8 M^{-1} s^{-1}, accelerated by an order of magnitude with respect to the same system in buffered aqueous solution. The photochemical quantum yield for water oxidation was 0.13, but the chemical yield of the system is significantly improved in comparison to the experiments made in pure aqueous buffered solution: in fact, CY is practically quantitative and photodecomposition of the sensitizer is minimized [48].

After the interesting results obtained with the Co_4O_4–H catalyst we investigated ligands modification in the cubane cluster in order to optimize photoinduced electron transfer (ET), photosynthetic yields, and quantum yields, while providing key descriptors of fundamental mechanistic aspects. Our approach was to focus on the diverse *para* substituted pyridines selected as terminal ligands of the cubane cluster, thus exerting a direct conjugation to each of the four cobalt sites.

To this end, the isostructural series with formula $[Co^{III}_4(\mu\text{-}O)_4(\mu\text{-}CH_3COO)_4(p\text{-}NC_5H_4X)_4]$, hereafter denoted Co_4O_4-X (X = Me, t -Bu, OMe, Br, COOMe, CN, Fig. 6) has been screened for WOC under illuminationand in the dark [48].

The impact of ligand substitution has been evaluated on (i) the electrocatalytic properties of the cobalt cubane, (ii) the rate of primary photoinduced ET events, and (iii) the photosynthetic performance for O_2 production. An unprecedented structure-reactivity analysis emerges herein, highlighting the importance of ET tuning within a photosynthetic sensitizer/catalyst system by stereoelectronic ligand modification.

The isostructural complexes are obtained according to literature protocols [38], and their solution identity and stability has been confirmed by NMR and ESI-MS. Inspection of the Co_4O_4-X catalyst properties has been initially addressed under dark conditions, with cyclic voltammetry (CV), by evaluating the water discharge overpotentials (η) and the onset of a catalytic current. These experiments confirm that Co_4O_4-X can actually perform water oxidation, with overpotentials varying in a narrow range (0.50–0.57 V, Table 2), but with no apparent ordering effect as a function of the pyridine substituent.

The impact of ligand substitution has been then explored under irradiation conditions, within the sacrificial $[Ru(bpy)_3]^{2+}/S_2O_8^{2-}$ cycle. In this system, photocatalytic turnovers are triggered by sequential "hole scavenging" events, involving consecutive ET steps from the cobalt cubane to photogenerated $[Ru(bpy)_3]^{3+}$ [16].

The primary ET rate is accessible through the flash photolysis technique. These experiments show that $[Ru(bpy)_3]^{3+}$ (whose formation is consistent with ground state bleaching at 450 nm, and, in the absence of an electron donor, is irreversible on the μs time scale) is reduced back to $[Ru(bpy)_3]^{2+}$ with kinetics dependent on the catalyst concentration as monitored by the absorbance increase at 450 nm. The bimolecular rate constant for the ET process can then be obtained, assuming pseudo-first order kinetic conditions, by linear

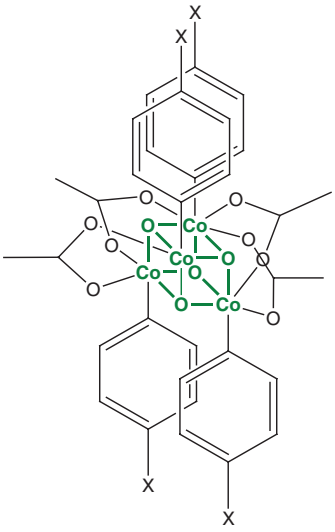

Fig. 6: A series of Co_4O_4–X cubanes (X = Me, t -Bu, OMe, Br, COOMe, CN) where the properties are tuned by substitution of the pyridine ligands in the para-position.

plots of rate constants *vs* catalyst concentration. For Co_4O_4-H in buffered water, primary ET was previously found to have a bimolecular rate constant, $k = (1.2–1.6) \times 10^7\ M^{-1}\ s^{-1}$ [39]. Under those conditions, however, the recovery of $[Ru(bpy)_3]^{2+}$ never reached completion in the flash photolysis experiments. This was mainly ascribed to a low thermodynamic driving force dictating the ET process in buffered water, where the redox couples $[Ru(bpy)_3]^{3+}/[Ru(bpy)_3]^{2+}$ and Co_4O_4-H^+/ Co_4O_4-H exhibit similar potentials (1.06 and 1.05 V, respectively, *vs* Ag/AgCl, NaCl 3 M) [39, 40]. The acceptor-donor redox gap can be remarkably enhanced in 1:1 CH_3CN/aqueous borate buffer (10 mM, pH 8), where the experimental potentials turn out to be 1.202 and 0.926 V, respectively.

The mixed solvent not only guarantees the proper thermodynamic boost for quantitative ET and complete recovery of the $[Ru(bpy)_3]^{2+}$ absorption, but also brings about a strong acceleration of the ET rate, with $k_H = 1.33 \times 10^8\ M^{-1}\ s^{-1}$, that is one order of magnitude higher than in buffered water (Table 2) [39].

In the mixed solvent, complete recovery of the $[Ru(bpy)_3]^{2+}$ absorption, in flash photolysis experiments, is obtained with all the isostructural Co_4O_4-X complexes.

Moreover, a remarkable ligand effect is observed on the ET kinetics as a function of the pyridine substituent, with k_X in the range $(0.14–2.51) \times 10^8\ M^{-1}\ s^{-1}$ (Table 1). In particular, a Hammett linear free energy relationship (LFER) is obtained by plotting log (k_X/k_H) *vs* the substituent σ constants (Fig. 7).

Table 2: Data for Co_4O_4-X catalysts.

X	η (V)[a]	K($10^8\ M^{-1}\ S^{-1}$)[b]	$E_{1/2}$ (mV)[c]	Φ (%)
OMe	0.57	2.51	877	40
Me	0.52	1.92	880	15
t-Bu	0.50	1.39	855	5
H	0.55	1.33	926	13
Br	0.53	0.60	990	16
COOMe	0.51	0.70	1040[d]	23
CN	0.51	0.14	1081[d]	13

[a]Overpotential of water discharge in 0.2 M phosphate buffer (pH 7), determined at an anode current value of 0.05 mA.
[b]Bimolecular rate constant for ET in CH_3CN: borate buffer 10 mM (1:1). [c]$E_{1/2}$ (Co_4O_4-X^+/Co_4O_4-X) in CH_3CN: borate buffer 10 mM (1:1). [d]$E_{1/2}$ (Co_4O_4-X^+/Co_4O_4-X) in CH_3CN: phosphate buffer 40 mM (1:1) since the wave in CH_3CN:borate buffer 10 mM (1:1) are not resolved due to the overlapping with water oxidation discharge.

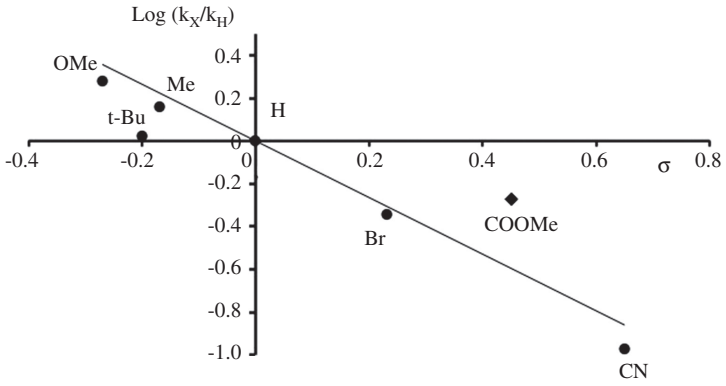

Fig. 7: Hammett linear free energy relationship plot of photoinduced ET rate constants.

The Hammett analysis provides a negative slope value, $\rho = -1.3$, indicating that photoinduced ET is favoured by electron-rich pyridine ligands. A similar approach has been previously reported in light-activated porphyrin dyads [49], but until now, the evidence that photoinduced ET is favoured by electron-rich pyridine ligands is unprecedented for photosynthetic assemblies involving multimetal cores. The crucial role of the ligands on the Co_4O_4 core confirmed its direct participation in photocatalytic activity for water oxidation.

While time-resolved spectroscopy reports on the first event of the photocatalytic cycle, the overall performance of the system is probed by evaluating (i) the oxygen production yield, (ii) the catalytic turnover number (TON), and (iii) the photochemical quantum yield (Φ).

In this aim, the oxygenic activity of the Co_4O_4-X series has been investigated in the presence of an excess of the $[Ru(bpy)_3]^{2+}/S_2O_8^{2-}$ couple. In a typical experiment, irradiation with an halogen lamp at $\lambda > 400$ nm of Co_4O_4-X (18 μM) in 1:1 CH_3CN: aqueous borate buffer (10 mM, pH 8) containing 1 mM $[Ru(bpy)_3]^{2+}$ and 5 mM $Na_2S_2O_8$ leads to continuous oxygen production with the time evolution profiles reported in Fig. 8 [48]. Under the conditions explored, the kinetics obey a zero order law, up to >80 % of persulfate consumption, most probably depending on the applied photon flux, which maintains a stationary state of photogenerated $[Ru(bpy)_3]^{3+}$. At variance with what was observed in aqueous buffer [39], in the mixed solvent, oxygen evolution occurs until quantitative consumption of the sacrificial electron acceptor, corresponding to a total of 140 turnovers for all Co_4O_4-X catalysts.

Such major improvement of the photosynthetic performance can result from an improved stability of the $[Ru(bpy)_3]^{2+}$ photosensitizer, as confirmed by UV- Vis spectra [48].

The most relevant descriptor addressing performance in photoinduced processes is, without doubt, the resulting photochemical quantum yield. The quantum yield values for the Co_4O_4-X catalysts, determined from

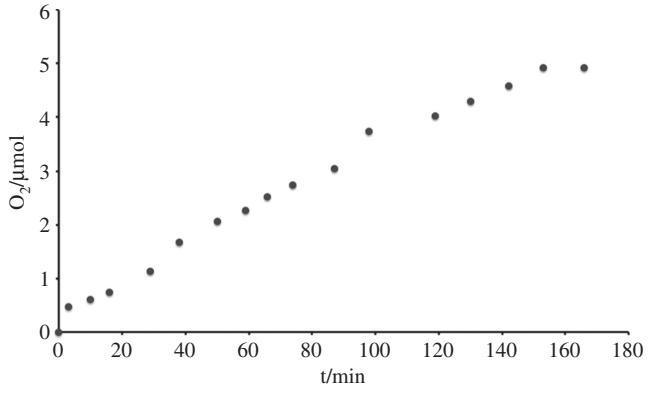

Fig. 8: Oxygen production kinetics by $[Co_4O_4$-COOMe$] = 18$ μM, $[Ru(bpy)_3^{2+}] = 1$ mM, $[S_2O_8^{2-}] = 5$ mM in 2 mL of 1:1 CH_3CN:borate buffer (10 mM, pH 8), $\lambda_{irr} > 400$ nm, with a 50 W halogen lamp.

the oxygen evolution rate over the first 30 min, are reported in Table 2. In particular, a record value of 40 % has been observed for Co_4O_4-OMe, setting a new benchmark in photoactivated water oxidation catalysis.

Unlike the primary ET process, the Φ trend does not show a straightforward dependence on the ligand electronic effect. The observed Φ order is as follows: OMe > COOMe > Me ≈ H ≈ Br ≈ CN > t-Bu (Table 2).

This result is probably related to an overall balance of competing factors crowning over diverse steps before oxygen release, and likely involving a multifaceted $Co^{III/IV}$ manifold. In particular, water coordination equilibria and the nucleophilic attack to metal-oxo intermediates, for O-O bond formation, are expected to be favored by electron-withdrawing ligands.

The final scenario is nevertheless converging on the supremacy of the Co_4O_4-OMe term, bringing about the fastest ET and the exceptional QY of 40 % determined for oxygen evolution under visible light irradiation (λ = 450 nm).

In the case of Co_4O_4-X, the strong impact observed upon subtle substituent changes in the periphery of the pyridine ligands is indicative of a molecular mechanism [47]. The natural course of evolution of this research is the incorporation of new helpful functions on this active WOC.

A functionalized tetracobalt(III) cubane as efficient molecular catalyst for light-driven water oxidation

Integration of molecular water oxidation catalysts into larger multicomponent systems, including electrodes or light-harvesting units, is highly desired for functional assemblies [50–52], however only very few attempts have been made so far to integrate such cobalt cubanes into larger, multicomponent systems [53, 54]. One such attempt is the preparation of a molecular triad made of the cobalt-oxo cubane $[Co_4O_4(CO_2Py)_2(bpy)_4]^{2+}$ (CO_2Py = 4-carboxypyridine) to which are coordinated, via the pyridine nitrogens, two $[Re(phen)(CO)_3]^+$ units (phen = 1,10-phenanthroline) [54].

Whereas photocatalytic properties of this triad versus photoinduced water oxidation were not reported, the integration of non-coordinated pyridine sites into the cubane structure opened the door to other, not yet pursued, to our knowledge, possibilities for inserting Co(III) cubanes into larger structures.

The synthetic tetracobalt(III) cubane, Co_4O_4-H proved to be quite efficient as a molecular water oxidation catalyst in the presence of $[Ru(bpy)_3]^{2+}$ as photosensitizer and sodium persulfate as sacrificial electron acceptor, as discussed before. The catalytic activity of Co_4O_4-H was maintained also in the presence of such substituents, not an obvious result, while the redox properties of the cubane system were finely tuned, thereby affecting the hole scavenging process and the overall photochemical quantum yield for water oxidation.

Here we report the synthesis and characterization of a new tetracobalt(III) cubane, Co_4O_4-H-ethynil benzoate, derived from Co_4O_4-H (Fig. 9) [75]. Differently from formerly-studied cubanes derived from Co_4O_4-H, substituted on the pyridines (Co_4O_4-X), in Co_4O_4-H-ethynil benzoate the substitution involves the acetate groups, each one carrying a phenyl-ethynyl moiety. The synthetic approach (vide infra) is also different from that used to prepare the above-mentioned cobalt cubane $[Co_4O_4(CO_2Py)_2(bpy)_4]^{2+}$, which is also substituted on the acetate groups with respect to its prototype $[Co_4O_4(CO_2Me)_2(bpy)_4]^{2+}$, from which it is directly prepared via a substitution reaction [38, 55, 56]. More interestingly, Co_4O_4-H-ethynil benzoate containsfour ethynyl groups, that point in different directions, and which can be used to graft Co_4O_4-H-ethynil benzoate onto various substrates (including surfaces) as well as for coupling Co_4O_4-H-ethynil benzoate with other molecular components (e.g., light-harvesting units). The redox behavior of Co_4O_4-H-ethynil benzoate and the photoinduced water oxidation properties of Co_4O_4-H-ethynil benzoate, in the presence of chromophores and sacrificial acceptors, are also investigated and compared with the properties of the prototype Co_4O_4-H. Results indicate that the functionalized Co_4O_4-H-ethynil benzoate keeps the useful catalytic properties of its prototype even in the presence of the ethynyl groups; in some cases, improved performance was found.

Co_4O_4-H-ethynil benzoate was prepared using the procedure employed for the synthesis of the prototype Co_4O_4-H [38, 55, 56]. The synthetic method, based on the designed cubane preparation from scratch, differs

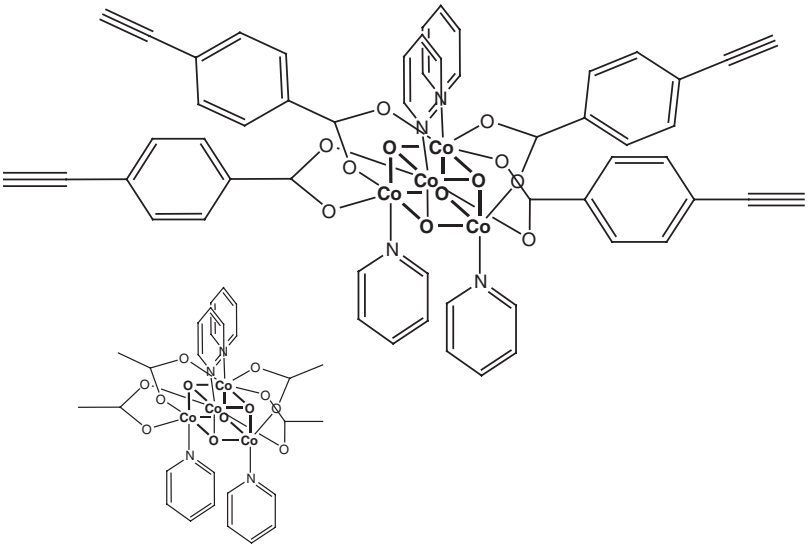

Fig. 9: Structural formula of Co_4O_4-H-ethynil benzoate. In the left-bottom corner, structural formula of Co_4O_4-H is also shown Reproduced from ref. [75] with permission of the Royal Society of Chemistry.

from the approach used for preparing various similar species with substituted acetate moieties [56], where the starting material was Co_4O_4-H itself. In our hands, preparing Co_4O_4-H-ethynil benzoate from the individual components gave better results than substitution of acetate units on the preformed cubane.

The absorption spectrum of Co_4O_4-H-ethynil benzoate in acetonitrile/phosphate buffer 1:1 (v/v) exhibits a very weak band at about 650 nm, followed by a more intense band at 355 nm.

The cyclic voltammograms of Co_4O_4-H-ethynil benzoate in mixed acetonitrile/aqueous buffered solution, are qualitatively similar to those of Co_4O_4-H: after a one-electron oxidation wave with $E_{1/2}$ at about 0.90 V, assigned to a quasi reversible Co(III) to Co(IV) oxidation, the catalytic water oxidation wave is present [39, 40, 48]. Also, the Co(III)/Co(IV) oxidation process occurs at approximately the same potential in Co_4O_4-H-ethynil benzoate and Co_4O_4-H, suggesting that substitution on the acetate bridging linkage minimally affects the redox properties of the cubane assembly – at least in the investigated conditions – with respect to substitution on the pyridines, which is known to produce significative shifts of the Co(III)/Co(IV) process [48].

Photoinduced water oxidation was investigated by using a sacrificial system containing $[Ru(bpy)_3]^{2+}$ (1×10^{-3} M), Co_4O_4-H-ethynil benzoate (1.87×10^{-5} M), and $Na_2S_2O_8$ (5 mM) in 2 mL of acetonitrile/phosphate buffer, exciting at $\lambda = 450$ nm [75].

The photochemical quantum yield, Φ, for molecular oxygen production, at $\lambda_{exc} = 450$ nm, was 0.36. This is a quite outstanding result and, considering the usual reaction scheme assumed to be valid in these type of systems [16, 40, 57–62], means that more than 70 % of photons absorbed by the photosensitizer are efficiently used to produce O_2. Such a quantum yield value is much larger than that reported for the prototype Co_4O_4-H under identical experimental conditions (0.13), thus indicating that the phenyl-ethynyl substituents on the acetate bridging ligands have a positive effect for the photocatalysis process. The reason for this behavior cannot be explained in the absence of mechanistic hypotheses, so this consideration should be regarded afor the moment as an experimental, but relevant, result.

Finally, the rate constant of hole scavenging, that is the electron transfer from the catalyst to the oxidized photosensitizer, has been investigated by flash photolysis. The bimolecular rate constant measured, 2.35×10^8 M^{-1} s^{-1}, is similar to that found for the same process involving Co_4O_4-H in identical experimental conditions, which is 1.88×10^8 M^{-1} s^{-1} in agreement with close similarity in CVs of Co_4O_4-H and Co_4O_4-H-ethynil benzoate [39, 40, 48].

However, as already found for the cobalt cubanes substituted on the pyridines, the rate constant of hole scavenging, although quite important for the system stability, is not the dominant factor affecting

photochemical quantum yield. In fact, in pyridine-substituted cobalt cubanes, Φ was not linearly correlated with hole scavenging rate constants, indicating that other factors, most likely intimately connected with the mechanism, were more important. Even in this case, in fact, the larger Φ value exhibited by Co_4O_4-H-ethynil benzoate is probably connected to successive steps in the overall water splitting mechanism.

The role of a vanadium species as catalyst in photo-induced water oxidation

Water oxidation catalysts containing earth-abundant metals like, not only, cobalt [39, 40] but also manganese [63–66], iron [67], and copper [68–70], have been studied. Surprisingly, in spite of the rich redox chemistry displayed by vanadium compounds [71, 72], not many vanadium species have been reported to behave as molecular water oxidation catalysts.

Recently, we reported photoinduced water oxidation obtained using a methoxo-polyoxovanadium cluster, namely $(N\text{-}Bu_4)[V_6O_7(OCH_3)_{12}]$ (V_6POM; Bu = n-C_4H_9), as the water oxidation catalyst [76]. It was the first time, to the best of our knowledge, that a vanadium species played the role of water oxidation catalyst. Moreover, whereas in most of the former reported polyoxometalate water oxidation catalysts the polyoxometalate unit(s) were mainly used as stabilizing units, with the catalytically-active metals not belonging to the polyoxometalate scaffold [18, 30, 31, 58, 61], in V_6POM the catalytically-active center is the polyoxometalate framework.

Compound V_6POM (see Fig. 10) was previously reported by Daniel and Hartl; [71, 72] it is a cluster formally derived from the highly symmetrical Lindqvist structure $[V_9O_{19}]^{n-}$ [73],where the 12 μ-bridged oxo ligands are substituted by methoxo ligands. Alkoxo-polyoxovanadium clusters similar to V_6POM exhibit a quite rich redox activity, with a series of thermodynamically stable redox isomers of general formula $[V^{IV}_{\ n}V^{V}_{\ 6-n}O_7(OR)_{12}]^{(4-n)}$ (R = alkyl groups), of which several species have been synthesized and characterized [71, 72]. In particular, compound 2 exhibits six one-electron redox processes in acetonitrile (although not all of them are reversible), in the potential window –1.0 ÷ +2.2 V vs. ferrocene/ferrocenium couple [72]. The absorption spectrum of each redox isomer has also been identified [72], evidencing the presence of intervalence bands, which allowed classification of the mixed-valence isomers as class II species, according to the Robin and Day formalism [74].

The photochemical quantum yield, Φ, for molecular oxygen production, investigated by using a sacrificial system made of $Ru(bpy)_3^{2+}$, V_6POM, and $Na_2S_2O_8$ in mixed solvent, and exciting with λ = 450 nm, was 0.20, indicating that 40 % of photons absorbed by the photosensitizer $Ru(bpy)_3^{2+}$ are efficiently used to produce O_2, assuming the generally accepted reaction scheme in which the sacrificial persulfate electron acceptor is the primary quencher (by irreversible electron transfer) of the metal-to-ligand charge-transfer excited state of $Ru(bpy)_3^{2+}$, with production of the oxidized sensitizer $Ru(bpy)_3^{3+}$, which successively undergoes a hole scavenging process with V_6POM. The sequence of above-mentioned individual steps is to be repeated several times, until the catalytically-active state of V_6POM is reached [19, 20]. This Φ value is quite promising when compared to that obtained for photochemical quantum yield of O_2 production using the cobalt(III) cubane-type species Co_4O_4-H, that is 0.13, under almost identical experimental conditions (the main difference was the presence of borate buffer, at pH 8, instead of the phosphate buffer, at pH 7, here used) [48].

As discussed above, an important parameter to determine the efficiency of a molecular catalyst in photoinduced water oxidation is the rate constant of hole scavenging, and a classical experiment for determining hole-scavenging rate constants is flash photolysis, in which $Ru(bpy)_3^{3+}$ is prepared by laser excitation of a $Ru(bpy)_3^{2+}$ solution, followed by irreversible oxidation of the metal-to-ligand charge-transfer (MLCT) state by persulfate anions. Formation of $Ru(bpy)_3^{3+}$ is indicated by the bleaching of the 450 nm MLCT absorption band, which in the absence of an electron donor, is irreversible on the μs timescale. In the presence of the molecular catalyst V_6POM, the bimolecular hole scavenging process takes place (eq. 12),

$$Ru(bpy)_3^{3+} + V_6POM \rightarrow Ru(bpy)_3^{2+} + V_6POM^{+} \quad (12)$$

by the absorbance difference changes observed at 450 nm (where $Ru(bpy)_3^{3+}$ and $Ru(bpy)_3^{2+}$ are the main absorbing species, and the process shows up as recovery of the initial bleach) and also at 405 nm (where the addi-

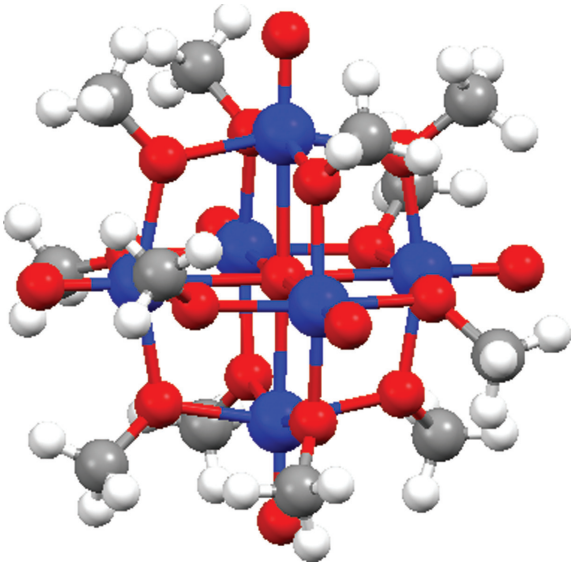

Fig. 10: Ball-and-stick representation of $[(V^{IV}_5V^{V}_1)O_7(OCH_3)_{12}]^-$ (counterion omitted for clarity; C, gray; H, white; O, red; V, blue).

tional positive absorption is indicative of the conversion of V_6POM to V_6POM$^+$). Using the conditions to ensure pseudo-first order kinetics, the rate constant for the hole scavenging reaction (eq. 12) was obtained as 2.5×10^8 M^{-1} s^{-1}. This rate constant is comparable to those obtained in similar conditions for a series of tetracobalt(III) cubane species formerly studied [48], and faster than for colloidal iridium oxide [29], widely considered to be a good water oxidation catalyst. Moreover, thanks to the difference between the absorption spectra of V_6POM and V_6POM$^+$ [72], oxidation of a molecular catalyst can be directly visualized and time-resolved in bimolecular systems in solution, although with limitation to the first oxidation step of the overall process.

Conclusions

An artificial photosynthetic system needs fundamental components such as antenna systems, reaction centres and multi electron transfer catalysts. The crucial step for the preparation of artificial photosynthetic systems is photo-induced water oxidation, in particular the development of efficient water oxidation catalysts (WOCs). A known efficient ruthenium catalyst, Ru_4POM, combined with a tetranuclear ruthenium dendrimer Ru_4dendrimer as photosensitizer, in a unique 4×4 ruthenium interplay, leads to an unprecedented photochemical quantum yield of 0.3 in sacrificial schemes containing persulfate anion acceptors. Considering the proposed mechanism of the photo-induced process, this means that 60 % of photons absorbed by the system were used to produce molecular oxygen from water. Interestingly, the Ru(II) dendrimer also works with low-energy photons, even at $\lambda > 550$ nm. So it was demonstrated that the ruthenium dendrimer, thanks to a broader absorption of solar light, is a better photosensitizer for photo-induced water oxidation system than the commonly used $[Ru(bpy)_3]^{2+}$.

The research for earth abundant elements used as WOCs led to investigation of different molecular cobalt cubane catalysts with formula $[Co^{III}_4(\mu\text{-}O)_4(\mu\text{-}CH_3COO)_4(p\text{-}NC_5H_4X)_4]$, Co_4O_4-X (X = Me, t-Bu, OMe, Br, COOMe, CN). These catalysts, which were synthetized and fully characterized, were combined with $[Ru(bpy)_3]^{2+}$ as photosensitizer in different experimental conditions. Ligand modification in the cubane cluster was made in order to optimize photoinduced electron transfer (ET) between the oxidized photosensitizer and the catalyst and photocatalytic performances. An unprecedented structure-reactivity analysis emerged, highlighting the importance of ET tuning within a photosynthetic sensitizer/catalyst system by stereoelectronic ligand modification.

A new, fully characterized, functionalized tetracobalt(III)-oxo cubane Co_4O_4–H-ethynil benzoate was prepared, using an unprecedented approach for the few formerly-studied, acetate-substituted cobalt cubanes. This species bears four peripheral ethynyl subunits; the presence of such subunits neither significantly affect the redox behavior of the species nor inhibits its catalytic properties *vs* water oxidation; on the contrary, it appears that the photochemical quantum yield for oxygen production from water in sacrificial systems based on Ru(II) polypyridine complexes and persulfate anions is larger (36 %) for Co_4O_4–H-ethynil benzoate with respect to the prototype species Co_4O_4–H (13 %). This result opens the way to the possibility of interfacing similar tetracobalt(III) cubane species with heterogeneous systems and/or molecular light-harvesting components, with the promise of retaining the useful catalytical properties of the cobalt cubane structure within the multicomponent assemblies.

Moreover, a multimetallic cluster containing vanadium atoms as the only transition metal centers has been demonstrated to play the role of water oxidation catalyst. The photochemical quantum yield (0.20) calculated using such methoxo-polyoxovanadate cluster as catalyst, using $Ru(bpy)_3^{2+}$ as the photosensitizer and $Na_2S_2O_8$ as the sacrificial electron acceptor is comparable with the quantum yield values obtained for the most studied homogeneous cobalt catalysts in similar photocatalytic systems. The rate constant for hole scavenging has been determined by following both the recovery of the photosensitizer $Ru(bpy)_3^{2+}$ and the formation of the oxidized molecular catalyst V_6POM^+. These results indicate that alkoxo-polyoxovanadium clusters are well-suited to take an active role in artificial photosynthetic schemes, and are expected to stimulate further work in the quest for molecular, active water oxidation catalysts made of less expensive, earth-abundant metals.

Acknowledgments: G.L.G. thanks Sebastiano Campagna for supervising her PhD thesis and for his support in this reseach project. Francesco Nastasi is acknowledged for his valuable collaboration in most of the research work here presented and Marie Pierre Santoni and Viviana Mollica Nardo are acknowledged for their contribution to some of the reviewed work. We wish also to thank Marcella Bonchio and Andrea Sartorel (University of Padova) for the great and long-standing collaboration in photocatalytic studies and for the design and preparation of most of the molecular WOCs here reported, and Franco Scandola and Mirco Natali (University of Ferrara) for the precious collaboration and the flash photolysis studies.

References

[1] N. S. Lewis, D. G. Nocera. *Proc. Natl. Acad. Sci. USA* **103**, 15729 (2006).
[2] N. D. McDaniel, S. Bernhard. *Dalton Trans.* **39**, 10021 (2010).
[3] M. G. Walter, E. I. Warren, J. R. McKone, S. W. Boettcher, Q. Mi, E. M. Santori, N. S. Lewis. *Chem. Rev.* **110**, 6446 (2010).
[4] H. B. Gray. *Nat. Chem*. **1**, 7 (2009).
[5] D. Gust, T. A. Moore, A. L. Moore. *Faraday Disc.* **155**, 9 (2012).
[6] J. H Alstrum-Acevedo, M. K. Brennaman, T. J. Meyer. *Inorg. Chem.* **44**, 6802 (2005).
[7] N. Armaroli, V. Balzani, N. Serpone. *Powering Planet Earth: Energy Solutions for the Future*, Wiley, New York (2012).
[8] R. Eisenberg, H. B. Gray. *Inorg. Chem.* **47**, 1697 (2008).
[9] D. G. Nocera. *Inorg. Chem.* **48**, 10001 (2009).
[10] J. J. Concepcion, R. L. House, J. M. Papanikolas, T. J. Meyer. *Proc. Natl. Acad. Sci. USA* **109**, 15560 (2012).
[11] J. P. McEvoy, G. W. Brudvig. *Chem. Rev.* **106**, 4455 (2006).
[12] H. Dau, I. Zaharieva. *Acc. Chem. Res.* **42**, 1861 (2009).
[13] L. Hammarstrom, S. Styring. *Energy Environ. Sci.* **4**, 2379 (2012).
[14] C. Herrero, A. Quaranta, W. Leibl, A. W. Rutherford, A. Aukauloo. *Energy Environ. Sci.* **4**, 2353 (2011).
[15] A. Sartorel, M. Bonchio, S. Campagna, F. Scandola. *Chem Soc. Rev.* **42**, 2262 (2013).
[16] F. Puntoriero, A. Sartorel, M. Orlandi, G. La Ganga, S. Serroni, M. Bonchio, Franco Scandola, S. Campagna. *Coord. Chem. Rev.* **255**, 2594 (2011).
[17] W. J. Youngblood, S.-H. A. Lee, Y. Kobayashi, E. A. Hernandez-Pagan, P. G. Hoertz, T. A. Moore, A. L. Moore, D. Gust, T. E. Mallouk. *J. Am. Chem. Soc.* **131**, 926 (2009).
[18] A. Sartorel, M. Carraro, F. M. Toma, M. Prato, M. Bonchio. *Energy Environ. Sci.* **5**, 5592 (2012).
[19] N. D. Morris, M. Suzuki, T. E. Mallouk. *J. Phys. Chem. A* **108**, 9115 (2004).

[20] P. G. Hoertz, Y.-I. Kim, W. J. Youngblood, T. E. Mallouk. *J. Phys. Chem. B* **111**, 6845 (2007).
[21] W. J. Youngblood, S. H. A. Lee, K. Maeda, T. E. Mallouk. *Acc. Chem. Res.* **42**, 1966 (2009).
[22] Y. V. Geletii, Z. Huang, Y. Hou, D. G. Musaev, T. Lian, C. L. Hill. *J. Am. Chem. Soc.* **131**, 7522 (2009).
[23] M. Orlandi, R. Argazzi, A. Sartorel, M. Carraro, G. Scorrano, M. Bonchio, F. Scandola. *Chem. Commun.* **46**, 3152 (2010).
[24] V. Balzani, A. Juris, M. Venturi, S. Campagna, S. Serroni. *Chem. Rev.* **96**, 759 (1996).
[25] S. Campagna, G. Denti, S. Serroni, A. Juris, M. Venturi, V, Ricevuto, V. Balzani. *Chem. Eur. J.* **1**, 211 (1995).
[26] M. H. V. Huynh, T. J. Meyer. *Chem. Rev.* **107**, 5004 (2007).
[27] V. Balzani, S. Campagna, G. Denti, A. Juris, S. Serroni, M. Venturi. *Acc. Chem. Res.* **31**, 26 (1998).
[28] S. Campagna, F. Puntoriero, F. Nastasi, G. Bergamini, V. Balzani. *Top. Curr. Chem.* **280**, 117 (2007).
[29] G. La Ganga, F. Nastasi, S. Campagna, F. Puntoriero. *Dalton Trans.* **45**, 9997 (2009).
[30] A. Sartorel, M. Carraro, G. Scorrano, R. De Zorzi, S. Geremia, N. D. McDaniel, S. Bernhard, M. Bonchio. *J. Am. Chem. Soc.* **130**, 5006 (2008).
[31] Y. V. Geletii, B. Botar, P. Köegerler, D. A. Hillesheim, D. G. Musaev, C. L. Hill. *Angew. Chem. Int. Ed.* **47**, 3896 (2008).
[32] A. Sartorel, P. Miró, E. Salvadori, S. Romain, M. Carraro, G. Scorrano, M. Di Valentin, A. Llobet, C. Bo, M. Bonchio. *J. Am. Chem. Soc*. **131**, 1605 (2009).
[33] M. Natali, M. Orlandi, S. Berardi, S. Campagna, M. Bonchio, A. Sartorel, F. Scandola. *Inorg. Chem.* **51**, 7324 (2012).
[34] L. Duan, L. Tong, Y. Xu, L. Sun. *Energy Environ. Sci*. **4**, 3296 (2011).
[35] Z. Huang, Z. Luo, Y. V. Geletii, J. W. Vickers, Q. Yin, D. Wu, Y. Hou, Y. Ding, J. Song, D. G. Musaev, C. L. Hill, T. Lian. *J. Am. Chem. Soc*. **133**, 2068 (2011).
[36] F. Puntoriero, G. La Ganga, A. Sartorel, M. Carraro, G. Scorrano, M. Bonchio, S. Campagna. *Chem. Commun*. **46**, 4725 (2010).
[37] E. A. Karlsson, B. L. Lee, T. Åkemark, E. V. Johnston, M. D. Karkas, J. L. Sun, O. Hansson, J. E. Backvall, B. Åkemark. *Angew. Chem. Int. Ed*. **50**, 11715 (2011).
[38] R. Chakrabarty, S. J. Bora, B. K. Das. *Inorg. Chem*. **46**, 9450 (2007).
[39] G. La Ganga, F. Puntoriero, S. Campagna, I. Bazzan, S. Berardi, M. Bonchio, A. Sartorel, M. Natali, F. Scandola. *Faraday Discuss*. **155**, 177 (2012).
[40] N. S. McCool, D. M. Robinson, J. E. Sheats, G. C. Dismukes. *J. Am. Chem. Soc*. **133**, 11446 (2011).
[41] M. W. Kanan, D. G. Nocera. *Science* **321**, 1072 (2008).
[42] E. M. P. Steinmiller, K. S. Choi. *Proc. Natl. Acad. Sci. USA* **106**, 20633 (2009).
[43] D. K. Zhong, D. R. Gamelin. *J. Am. Chem. Soc*. **132**, 4202 (2010).
[44] S. Y. Reece, J. A. Hamel, K. Sung, T. D. Jarvi, A. J. Esswein, J. J. H. Pijpers, D. G. Nocera. *Science* **334**, 645 (2011).
[45] P. K. Ghosh, B. S. Brunschwig, M. H. Chou, C. Creutz. N. Sutin. *J. Am. Chem. Soc*. **106**, 4772 (1984).
[46] M. Hara, C. C. Waraksa, J. T. Lean, B. A. Lewis, T. E. Mallouk. *J. Phys. Chem. A* **104**, 5275 (2000).
[47] J. G. McAlpin, Y. Surendranath, M. Dinca, T. A. Stich, S. A. Stoian, W. H. Casey, D. G. Nocera, R. D. Britt. *J. Am. Chem. Soc*. **132**, 6882 (2010).
[48] S. Berardi, G. La Ganga, M. Natali, I. Bazzan, F. Puntoriero, A. Sartorel, F. Scandola, S. Campagna, M. Bonchio. *J. Am. Chem. Soc*. **134**, 11104 (2012).
[49] D. Gust, T. A. Moore, A. L. Moore, H. K. Kang, J. M. DeGraziano, P. A. Liddell, G. R. Seely. *J. Phys. Chem.* **97**, 13637 (1993).
[50] J. R. Swierk, T. J. Mallouk. *Chem. Soc. Rev.* **42**, 2357 (2013).
[51] L. Alibabaei, H. Luo, T. L. House, P. G. Hoertz, R. Lopez, T. J. Meyer. *J. Mater. Chem. A* **1**, 4133 (2013).
[52] R. Abe. *J. Photochem. Photobiol. C: Photochem. Rev*. **11**, 179 (2010).
[53] B. Zhang, F. Li, F. Yu, X. Wang, X. Zhou, H. Li, Y. Jiang, L. Sun. *ACS Catal.* **4**, 804 (2014).
[54] M. D. Symes, D. A. Lutterman, T. S. Teets, B. L. Anderson, J. J. Breen, D. G. Nocera. *ChemSusChem*, **6**, 65 (2013).
[55] J. K. Beattie, T. W. Hamblie, J. A. Klepetko, A. F. Masters, P. Turner. *Polyhedron* **17**, 1343 (1998).
[56] R. Chakrabarty, P. Sarmah, B. Saha, S. Chakravorty, B. K. Das. *Inorg. Chem.* **48**, 6371 (2009).
[57] V. Artero, M. Chavarot-Kerlidou, M. Fontecave. *Angew. Chem. Int. Ed.* **50**, 7238 (2011).
[58] S. Tanaka, M. Annaka, K. Sakai. *Chem. Commun.* **48**, 1653 (2012).
[59] D. J. Wasylenko, R. D. Palmer, E. Schott, C. P. Berlinguette. *Chem. Commun.* **48**, 2107 (2012).
[60] F. Song, Y. Ding, B. Ma, C. Wang, Q. Wang, X. Du, S. Fu. *J. Energy Environ. Sci.* **6**, 1170 (2013).
[61] J. J. Stracke, R. G. Finke. *ACS Catal.* **4**, 79 (2014).
[62] P. F. Smith, C. Kaplan, J. E. Sheats, D. M. Robinson, N. S. McCool, N. Mezle, G. C. Dismukes. *Inorg. Chem.*, **53**, 2113 (2014).
[63] R. K. Hocking, R. Brimblecombe, L. Y. Chang, A. Singh, M. H. Cheah, C. Glover, W. H. Casey, L. Spiccia. *Nat. Chem*. **3**, 461 (2011).
[64] W. C. Ellis, N. D. McDaniel, S. Bernhard, T. J. Collins. *J. Am. Chem. Soc.* **132**, 10990 (2010).
[65] J. L. Fillol, Z. Codolà, I. Garcia-Bosch, L. Gòmez, J. J. Pla, M. Costas. *Nat. Chem.* **3**, 807 (2011).
[66] G. Chen, L. Chen, S. M. Ng, W. L. Man, T. C. Lau. *Angew. Chem. Int. Ed.* **52**, 1789 (2013).
[67] S. M. Barnett, K. I. Goldberg, J. M. Mayer. *Nat. Chem.* **4**, 498 (2012).
[68] V. G. Kessler, G. A. Seisenbaeva. *Inorg. Chem. Commun.* **3**, 203 (2000).
[69] J. Spandl, C. Daniel, I. Brüdgam, H. Hartl. *Angew. Chem., Int. Ed.* **42**, 1163 (2003).
[70] M. J. Shaw. *Vanadium Electrochemistry, Encyclopedia of Electrochemistry*, Wiley, Weinheim (2007).

[71] C. Daniel, H. Hartl. *J. Am. Chem. Soc.* **127**, 13978 (2005).
[72] C. Daniel, H. Hartl. *J. Am. Chem. Soc.* **131**, 5101 (2009).
[73] I. Lindqvist. *Ark. Kemi* **5**, 247 (1953).
[74] M. P. Robin, P. Day. *Adv. Inorg. Chem. Radiochem.* **10**, 247 (1967).
[75] G. La Ganga, V. Mollica Nardo, M. Cordaro, M. Natali, S. Vitale, A. Licciardello, F. Nastasi, S. Campagna. *Dalton Trans.* **43**, 14926 (2014).
[76] M. P. Santoni, G. La Ganga, V. Mollica Nardo, M. Natali, F. Puntoriero, F. Scandola, S. Campagna. *J. Am. Chem. Soc.* **136**, 8189 (2014).